Polarized Spectra and Crystal-Field Parameters of Eu^{+3} in YVO_4

C. BRECHER, H. SAMELSON, A. LEMPICKI, R. RILEY, AND T. PETERS
The Bayside Laboratory, Research Center of General Telephone and Electronics Laboratories Inc., Bayside, New York

(Received 25 August 1966)

The polarized emission and absorption spectra of single crystals of yttrium vanadate doped with Eu^{+3} were measured and analyzed. The spectra are consistent with the D_{2d} site symmetry of the Eu^{+3} ion in this lattice, and no significant violation of the appropriate electric- and magnetic-dipole selection rules is found. Most of the observed transitions are identified, and the complete energy-level structure of the ion has been defined for all states below the $^5D_3$. A crystal-field model has been used to describe the structure of the ^7F multiplet. The requisite crystal-field parameters have been ascertained and the energies of the various Stark levels calculated. The simple electrostatic field approximation is found to give an adequate description of the experimental data, but the necessity for a more refined treatment is indicated.

INTRODUCTION

THE spectroscopy of tripositive europium has been of considerable interest in the study of the coordination properties of rare-earth ions. The major features of the energy-level structure have been well established,[1–3] and the emission characteristics of this ion have been investigated in a wide range of host materials. Much useful information has been obtained from studies of liquids and powdered solids,[4,5] but measurements on single crystals, with the characteristic polarization properties of the ion emissions and absorptions, have yielded the most unambiguous results.[6–9] In addition, the energy-level structure of the ion in a number of hosts has been analyzed in terms of an electrostatic crystal-field model,[8–11] and some progress has been made in the interpretation of the influences exerted upon the ion by the arrangement of its immediate neighbors.

Of the many possible arrangements of the immediate environment, those most preferred by the europium ion are octacoordinate. Theoretical treatment of such coordination has not been extensive and is almost invariably limited to cubic arrangements or those deviating only slightly from cubic. However, most eightfold coordinations manifest a tetragonal or lower symmetry, deviating substantially from the isotropic cases normally considered. It is one of the purposes of these investigations to develop the crystal-field treatment for such tetragonal symmetries and to examine its application to a number of real systems.

Eightfold coordination is physically realized by the europium ion in a number of different forms: in the solvated ion, in molecular chelates, and in inorganic crystalline lattices. One such suitable lattice structure is of the zircon type, which can be described by the general formula $M^{+m}N^{+(8-m)}O_4$, where M and N are metal ions having coordination numbers of eight and four, respectively. One member of this class of crystals, yttrium vanadate (YVO_4), has been of particular recent interest because of its intense cathodoluminescence when it is doped with europium.[12] Single crystals of this material proved to be nearly ideal for the investigation of the polarized spectra of trivalent europium in a tetragonal octacoordinate site. This paper reports the results of such an investigation and discusses these results in terms of an electrostatic crystal-field model.

EXPERIMENTAL

Materials

All the crystals used in this work were produced by growth from a suitable flux, consisting of either molten V_2O_5 or $Na_4V_2O_7$. In both cases the material was given an equilibration soak at 1200°C, followed by cooling at the rate of 10°C/h with the V_2O_5 flux and 2°C/h with $Na_4V_2O_7$. These solutions tend to nucleate easily, and the supersaturation must be carefully controlled to provide crystals of reasonable size and good optical quality. After cooling several hundred degrees, the liquid flux was poured off and the crystals leached with 5% sodium carbonate until free of encrusted solvent. The resultant crystals contained 1 to 4 mole % europium, approximately half of the concentration of europium initially added. The sizes varied, but many were in the form of flat plates 1 to 3 mm on edge and 0.1 to 0.8 mm thick. The crystals were uniaxial and had their unique axis in the plane of the plate and parallel to one pair (usually the long pair) of edges. In the polarizing microscope very sharp extinctions were observed when the light was propagated perpendicular to the unique axis. With light propagated along the unique axis, the crystals were isotropic. For optical measurements the

[1] G. Joos and K. H. Hellwege, Ann. Physik **39**, 25 (1941).
[2] K. H. Hellwege, Nachr. Akad. Wiss. Goettingen, Math-Physik, Kl. **1947**, 37 (1947).
[3] B. R. Judd, Proc. Roy. Soc. (London) **A228**, 120 (1955).
[4] H. Gobrecht, Ann. Physik **28**, 673 (1937).
[5] B. Rinck, Z. Naturforsch. **3**, 406 (1948).
[6] K. H. Hellwege, Ann. Physik **4**, 95 (1948); **4**, 127 (1948); **4**, 136 (1948); **4**, 143 (1948); **4**, 357 (1949).
[7] E. V. Sayre and S. Freed, J. Chem. Phys. **24**, 1213 (1955).
[8] L. G. DeShazer and G. H. Dieke, J. Chem. Phys. **38**, 2190 (1963).
[9] J. A. Koningstein, Phys. Rev. **136**, A717 (1964); J. Chem. Phys. **42**, 3195 (1965).
[10] B. R. Judd, Mol. Phys. **2**, 407 (1959).
[11] J. Briffaut, Compt. Rend. **262**, 562 (1966).
[12] A. K. Levine and F. C. Palilla, Appl. Phys. Letters **6**, 118 (1964).

plane faces were invariably suitable without further treatment, but both other sets of faces had to be ground and polished. Six crystals from both methods of preparation were studied in survey and all yielded precisely the same spectra. The largest one, from the $Na_4V_2O_7$ flux, was studied in detail, and the results reported are those obtained on this crystal.

Measurements

Three distinct types of spectroscopic measurements were made on the material: visible emission, visible absorption, and infrared absorption. The first two were made with a Jarrell-Ash 0.5-m Ebert monochromator with circular slits, and detected with an ITT FW130 photomultiplier having an S-20 surface. The crystals were mounted in a holder contained within a Dewar apparatus and bathed in a regulated stream of dry nitrogen gas maintained at the desired temperatures, usually 25 and $-180°C$ for most of these experiments. The excitation source for the emission was an HBO 200 Hg lamp whose output was filtered through Schott UG1 and UG11 filters; for the absorption a G.E. 6-V tungsten-ribbon-filament lamp was used. Straight-through optics were employed, and in both cases, the light from the crystal was passed through a rotatable polarizer before entering the monochromator.

Spectra were recorded with the light propagated along the crystallographic c axis (the axial spectrum) and with the light propagated transverse to this axis. In the latter case the polarization was determined with the electric vector parallel to the c axis (the π spectrum) and perpendicular to the c axis (the σ spectrum). For the infrared-absorption measurements, no polarized spectra were taken, but, as in the previous cases, spectra were taken both with the light propagated along the crystallographic c axis and propagated perpendicular to it.

The locations of some of the pertinent optical transitions are given in Tables I–III. The infrared spectra were recorded between 500 and 4000 cm^{-1} using a Perkin-Elmer 421 grating spectrophotometer, and between 4000 and 6000 cm^{-1} with a Cary-14 spectrophotometer. Visible absorption was recorded between 4000 and 6000 Å, and visible emission between 4000 and 8500 Å. These respective spectra are shown in Figs. 1–7.

DISCUSSION

Spectroscopy

Yttrium vanadate is an excellent inorganic host medium for trivalent europium. Aside from the conveniences of clarity, hardness, and chemical inertness, this material has an ionic lattice with the desirable property of providing europium with a trivalent site in which it can reside without the necessity of chemical charge compensation. In addition, the elements of the local (or short-range) symmetry governing the ion emission and absorption coincide with the crystallographically determined lattice symmetry elements, thus minimizing spectroscopic ambiguity.

Some x-ray information is available for yttrium vanadate.[13,14] The lattice, a typical zircon structure, is tetragonal, belonging to space group D_{4h}^{19}-$I4/amd$, and has unit cell dimensions of $c=6.27$ Å and $a=7.10$ Å. The europium ion, which enters the lattice substitutionally in yttrium sites, is surrounded by eight oxygens at the vertices of a tetragonal dodecahedron. The local site symmetry of the ion is D_{2d}.

The emission characteristics from europium in this sort of structure are simple and straightforward. All transitions, be they magnetic or electric dipole, must fall along one of two directions: either along the unique crystallographic c axis (nondegenerate transitions) or perpendicular to this axis (doubly degenerate transitions). Thus, when the crystal is oriented so that the cross section viewed by the monochromator is the isotropic plane (that is, with the emitted light propagated along the c axis), only the degenerate transitions will appear in the spectrum. With these transitions identified unequivocally, spectra taken with the emitted light propagated perpendicular to the c axis will reveal the nondegenerate transitions. Analysis of the emitted light through a polarizer confirms the identification and distinguishes between magnetic- and electric-dipole radiation mechanisms. Similar considerations prevail for visible absorptions involving the same transitions.

In addition to the emission and absorption spectra of transitions between the $^5D_0$ states and various levels in the ^7F ground multiplet, certain transitions within the latter multiplet itself can be measured directly by infrared absorption. The absorptions between 1900 and 6000 cm^{-1} correspond to the $^7F_0$-$^7F_3$, $^7F_0$-$^7F_4$, $^7F_0$-$^7F_5$, $^7F_0$-$^7F_6$, $^7F_1$-$^7F_4$, and $^7F_1$-$^7F_5$ transitions, of which the latter two cannot be observed in the low-temperature spectrum. Unfortunately, the lower-energy transitions in the ^7F multiplet cannot be directly observed in this manner because of the interference of the lattice absorption bands below 1900 cm^{-1}. Indeed, not all of the levels in the ^7F multiplet can be measured directly since many transitions do not fall in active representations; these, however, can usually be found algebraically from combinations of the frequencies of other allowed transitions.

The identification of the energy levels depends on two well-established facts: (1) that the spin-orbit coupling is sufficiently strong that only the total angular momentum J is a good quantum number; and (2) that the crystal-field splitting is considerably less than the spin-orbit splitting, and operates on the J number of the individual spin-orbit levels. The selection rules for the electromagnetic transitions in dodecahedral symmetry are summarized in Table IV, while the distribution of

[13] W. O. Milligan and L. W. Vernon, J. Phys. Chem. **56**, 145 (1952).
[14] E. Broch, Z. Physik Chem. **20B**, 345 (1932).

TABLE I. Fluorescent emissions from europium-doped yttrium vanadate (at −180°C).

Wavelength (Å)	Energy (cm^{-1})	Relative intensity range[a]	Polarization[b]	Assignment
4614	21 673	3	π	
4661	21 455	4	π	$^5D_2(B_2)$ -$^7F_0(A_1)$
4673	21 400	5	σ,α	$^5D_2(E)$ -$^7F_0(A_1)$
4678	21 377	3	π	
4704	21 261	3	π	
4705	21 256	4	σ,α	
4714	21 213	3	σ,α	
4743	21 084	4		$^5D_2(B_1)$-$^7F_1(A_2)$
4775	20 944	3		
4783	20 907	3	π	
4794	20 859	2		
4801	20 829	4	σ,α	
4815	20 768	3	π	
4842	20 653	5		
4848	20 627	4	π	
4852	20 610	3	π	
4907	20 379	2		$^5D_2(B_1)$-$^7F_2(E)$
4912	20 358	3	π	$^5D_2(E)$ -$^7F_2(E)$
4922	20 319	3	σ,α	$^5D_2(A_1)$-$^7F_2(E)$
4926	20 300	3	π	
4942	20 236	1	π	
5279	18 942	4	π,α	$^5D_1(E)$ -$^7F_0(A_1)$
5282	18 932	4	σ	$^5D_1(A_2)$-$^7F_0(A_1)$
5375	18 605	7	σ,α	$^5D_1(E)$ -$^7F_1(A_2)$
5386	18 566	7	π	$^5D_1(E)$ -$^7F_1(E)$
5389	18 556	7	σ,α	$^5D_1(A_2)$-$^7F_1(E)$
5392	18 546	5	σ,α	
5540	18 051	3	π	
5554	18 005	5	σ,α	$^5D_1(E)$ -$^7F_1(E)$
5558	17 991	4		
5569	17 957	5	σ,α	$^5D_1(E)$ -$^7F_2(A_1)$
5573	17 944	4	σ	$^5D_1(A_2)$-$^7F_2(A_1)$
5576	17 934	4	σ,α	
5586	17 902	5	σ	$^5D_1(E)$ -$^7F_2(E)$
5589	17 892	5	π,α	$^5D_1(A_2)$-$^7F_2(E)$
5610	17 825	3	π,α	$^5D_1(E)$ -$^7F_2(B_1)$
5613	17 816	5	π	$^5D_1(A_2)$-$^7F_2(B_1)$
5632	17 755	3	π	
5709	17 515	2		$^5D_2(B_2)$-$^7F_5(E^{(1)})$
5717	17 491	5	σ,α	$^5D_2(A_1)$-$^7F_5(E^{(3)})$
5724	17 470	6	σ,α	$^5D_2(E)$ -$^7F_5(B_2)$ $^5D_2(B_1)$-$^7F_5(E^{(1)})$
5731	17 449	4		$^5D_2(E)$ -$^7F_5(E^{(1)})$
5738	17 428	4	π	$^5D_2(A_1)$-$^7F_5(B_2)$
5741	17 419	4	σ,α	$^5D_2(A_1)$-$^7F_5(E^{(1)})$
5746	17 404	6		
5753	17 382	6	π	
5761	17 359	3	π	
5777	17 310	6	σ,α	$^5D_2(E)$ -$^7F_5(B_1)$
5784	17 288	5		
5790	17 271	4	σ,α	
5819	17 183	1	(powder)	$^5D_0(A_1)$-$^7F_0(A_1)$
5854	17 083	6	σ,α	$^5D_1(E)$ -$^7F_3(B_2)$
5859	17 068	6	σ,α	$^5D_1(E)$ -$^7F_3(A_2)$
5869	17 039	6	σ,α	$^5D_1(E)$ -$^7F_3(B_1)$
5873	17 027	8	π	$^5D_1(A_2)$-$^7F_3(B_1)$
5874	17 025	4	α	$^5D_1(A_2)$-$^7F_3(E^{(2)})$
5888	16 983	6	π	$^5D_1(E)$ -$^7F_3(E^{(1)})$
5891	16 975	6	σ,α	$^5D_1(A_2)$-$^7F_3(E^{(1)})$
5913	16 912	4	π	
5918	16 898	4		
5935	16 849	9	σ	$^5D_0(A_1)$-$^7F_1(A_2)$
5937	16 844	6		
5950	16 807	9	π,α	$^5D_0(A_1)$-$^7F_1(E)$
5953	16 798	7		
5961	16 775	3		
5983	16 712	5		
6036	16 567	5		
6044	16 545	5		$^5D_2(B_2)$-$^7F_6(E^{(3)})$
6064	16 491	4	σ,α	$^5D_2(B_1)$-$^7F_6(E^{(3)})$
6097	16 401	8	π	$^5D_2(A_1)$-$^7F_6(B_2^{(1)})$
6109	16 369	7	π	$^5D_2(B_1)$-$^7F_6(A_2)$
6117	16 347	5	σ,α	$^5D_2(B_1)$-$^7F_6(E^{(1)})$ $^5D_2(E)$ -$^7F_6(A_2)$
6133	16 305	8	π	$^5D_2(E)$ -$^7F_6(E^{(1)})$
6155	16 246	10	π	$^5D_0(A_1)$-$^7F_2(B_2)$
6161	16 232	8	π	$^5D_1(A_2)$-$^7F_4(B_1)$
6194	16 145	10	σ,α	$^5D_0(A_1)$-$^7F_2(E)$
6226	16 062	6	σ,α	$^5D_1(E)$ -$^7F_4(A_1^{(2)})$
6243	16 018	7	σ,α	$^5D_1(E)$ -$^7F_4(A_2)$
6269	15 952	6	π	$^5D_1(E)$ -$^7F_4(E^{(1)})$
6273	15 941	5		$^5D_1(A_2)$-$^7F_4(E^{(1)})$
6298	15 878	7	σ,α	$^5D_1(E)$ -$^7F_4(A_1^{(1)})$
6352	15 743	5	π	
6376	15 684	5	σ,α	
6404	15 615	3		
6444	15 519	4		
6468	15 460	6	σ,α	
6487	15 415	8	π	
6513	15 354	7		
6516	15 347	6	σ,α	
6524	15 318	8	π	$^5D_0(A_1)$-$^7F_3(B_2)$
6532	15 310	6		
6545	15 279	7	σ,α	$^5D_0(A_1)$-$^7F_3(E^{(2)})$
6554	15 208	6		
6567	15 227	7	σ,α	$^5D_0(A_1)$-$^7F_3(E^{(1)})$
6583	15 190	3	σ,α	$^5D_1(E)$ -$^7F_5(A_2^{(2)})$
6605	15 140	3	σ,α	$^5D_1(E)$ -$^7F_5(A_1)$
6629	15 085	4	σ,α	$^5D_1(E)$ -$^7F_5(A_2^{(1)})$
6633	15 076	2		$^5D_1(E)$ -$^7F_5(E^{(3)})$
6640	15 060	4	σ,α	$^5D_1(A_2)$-$^7F_5(E^{(3)})$
6647	15 044	4	π	
6654	15 028	5	σ,α	$^5D_1(E)$ -$^7F_5(B_2)$
6659	15 017	3		$^5D_1(E)$ -$^7F_5(E^{(2)})$
6668	14 997	3		$^5D_1(E)$ -$^7F_5(E^{(1)})$
6673	14 986	5	σ,α	$^5D_1(A_2)$-$^7F_5(E^{(1)})$
6728	14 865	4	π	$^5D_1(A_2)$-$^7F_5(B_1)$
6771	14 769	5	π	
6814	14 676	5	σ,α	
6968	14 351	2		$^5D_0(A_1)$-$^7F_4(E^{(2)})$
6986	14 315	9	π	$^5D_0(A_1)$-$^7F_4(B_2)$
7045	14 194	9	σ,α	$^5D_0(A_1)$-$^7F_4(E^{(1)})$
8119	12 317	6	π	$^5D_0(A_1)$-$^7F_6(B_2^{(2)})$
8152	12 267	6	σ,α	$^5D_0(A_1)$-$^7F_6(E^{(3)})$
8172	12 237	6	π	$^5D_0(A_1)$-$^7F_6(B_2^{(1)})$

[a] The emission intensities of all transitions were normalized to constant spectroscopic conditions, to correct for differences in detector sensitivity, slit width, etc. These were divided by the intensity of the strongest line, and averaged over the three crystal directions. Finally, the results were segregated on a logarithmic basis into semidecades, with the most intense group given the value of 10 and two units denoting a change of one order of magnitude.

[b] The polarization characteristics of the light relative to the unique crystallographic axis are expressed always in terms of the plane of the *electric* vector in the following manner: σ (transverse), propagation direction perpendicular to the unique axis, electric vector also perpendicular to it; π (transverse), propagation direction perpendicular to the unique axis, but electric vector parallel to it; and α (axial), propagation direction parallel to the unique axis, electric vector unpolarized. The polarization characteristics of a particular transition are reported above only if the respective σ and π intensities differ by more than a factor of 2.

TABLE II. Visible absorptions of europium-doped yttrium vanadate.

Wavelength (Å)	Energy (cm^{-1})	Temperature of measurement (°C)	Relative intensity range[a]	Polarization[a]	Assignment
4661	21 455	−180	10	π	$^5D_2(B_2)$-$^7F_0(A_1)$
4675	21 392	−180	10	σ,α	$^5D_2(E)$ -$^7F_0(A_1)$
4743	21 085	+25	8	π	$^5D_2(B_1)$-$^7F_1(A_2)$
4748	21 062	+25	8	σ,α	$^5D_2(E)$ -$^7F_1(A_2)$
4752	21 045	+25	8	σ,α	$^5D_2(B_1)$-$^7F_1(E)$
4757	21 023	+25	8	π	$^5D_2(E)$ -$^7F_1(E)$
4766	20 983	+25	8	σ,α	$^5D_2(A_1)$-$^7F_1(E)$
5280	18 940	−180	9	π,α	$^5D_1(E)$ -$^7F_0(A_1)$
5283	18 930	−180	9	σ	$^5D_1(A_2)$-$^7F_0(A_1)$
5376	18 605	+25	8	σ,α	$^5D_1(E)$ -$^7F_1(A_2)$
5387	18 564	+25	8	π	$^5D_1(E)$ -$^7F_1(E)$
5390	18 554	+25	8	σ,α	$^5D_1(A_2)$-$^7F_1(E)$
5936	16 847	+25	8	σ	$^5D_0(A_1)$-$^7F_1(A_2)$
5951	16 805	+25	8	π,α	$^5D_0(A_1)$-$^7F_1(E)$

[a] The polarization and relative intensity are reported in the same manner as in Table I, except for the use of absorbance in place of emission.

the splittings among the various representations of this symmetry group can be found in Table V.

Probably the most precisely defined state in this investigation is the $^5D_1$ since the transitions between it and the ground state were measured in both emission and absorption. This $^5D_1$-$^7F_0$ transition consists of two components, a doubly degenerate one at 5279 Å and a nondegenerate one at 5282 Å. Both are active as magnetic dipoles, as confirmed by their polarization behavior, and locate the two $^5D_1$ levels at 18 932.0 and 18 941.0 cm^{-1}, the latter doubly degenerate.

The $^5D_2$ state can be located, in part, by the same technique. Two components of the $^5D_2$-$^7F_0$ transition can be found in both emission and absorption, at 4661 and 4674 Å; from their polarization behavior the nondegenerate B_2 level is located at 21 455 cm^{-1} and the degenerate E level at 21 396 cm^{-1}. In this case, however, the other two of the four Stark levels of the state cannot be so found, since the transitions between them and ground are not optically active. These levels (A_1 and B_1) can be located from other transitions, particularly from absorptions originating in the $^7F_1$ state at elevated temperatures; however, because the levels shift as much as 5 cm^{-1} with temperature, this information is only of limited usefulness for the purposes of this study.

The $^5D_0$ level is the only member of the ^5D multiplet that cannot be measured directly, since the site symmetry forbids any optical activity for the $^5D_0$-$^7F_0$ transitions. The $^5D_0$ state, however, is the initial level in the most intense fluorescent transitions, and must be located precisely if the ^7F levels are to be determined. This is accomplished by using the $^5D_1$-$^7F_1$ emissions to ascertain the locations of the $^7F_1$ levels, and then using the $^5D_0$-$^7F_1$ emissions to fix the $^5D_0$ level. The $^5D_1$-$^7F_1$ transition is active as an electric dipole with one emission at 5386 Å, polarized along the c axis, and two, at 5375 and 5389 Å, polarized perpendicular to the c axis; these locate the A_2 and E levels of the $^7F_1$ state at 375.6

TABLE III. Infrared absorptions of europium-doped yttrium vanadate.

Energy (cm^{-1})	Temperature of measurement (°C)	Relative intensity range[a]	Polarization[a]	Assignment
1905	−180	7	σ,α	$^7F_3(E^{(2)})$-$^7F_0(A_1)$
1955	−180	7	σ,α	$^7F_3(E^{(1)})$-$^7F_0(A_1)$
2365	+25	7	π	$^7F_4(B_1)$ -$^7F_1(A_2)$
2450	+25	7	π	$^7F_4(E^{(2)})$-$^7F_1(E)$
2495	+25	9	σ,α	$^7F_4(B_2)$ -$^7F_1(E)$ $^7F_4(E^{(2)})$-$^7F_1(A_2)$
2550	+25	7	σ,α	$^7F_4(A_2)$ -$^7F_1(E)$
2612	+25	8	π	$^7F_4(E^{(1)})$-$^7F_1(E)$
2660	+25	8	σ,α	$^7F_4(E^{(1)})$-$^7F_1(A_2)$
2830	−180	7	σ,α	$^7F_4(E^{(2)})$-$^7F_0(A_1)$
2868	−180	9	π	$^7F_4(B_2)$ -$^7F_0(A_1)$
2988	−180	10	σ,α	$^7F_4(E^{(1)})$-$^7F_0(A_1)$
3538	+25	8	σ,α	$^7F_5(B_2)$ -$^7F_1(E)$ $^7F_5(E^{(3)})$-$^7F_1(A_2)$
3575	+25	8	π	$^7F_5(E^{(1)})$-$^7F_1(E)$
3615	+25	7	σ,α	$^7F_5(E^{(1)})$-$^7F_1(A_2)$
3640	+25	6		
3690	+25	8	σ,α	$^7F_5(B_1)$ -$^7F_1(E)$
3730	+25	8	π	$^7F_5(B_1)$ -$^7F_1(A_2)$
3750	−180	6		
3870	−180	9	σ,α	$^7F_5(E^{(3)})$-$^7F_0(A_1)$
3915	−180	7	π	$^7F_5(B_2)$ -$^7F_0(A_1)$
3928	−180	8	σ,α	$^7F_5(E^{(2)})$-$^7F_0(A_1)$
3949	−180	9	σ,α	$^7F_5(E^{(1)})$-$^7F_0(A_1)$
4746	−180	7	π	
4867	−180	10	π	$^7F_6(B_2^{(1)})$-$^7F_0(A_1)$
4916	−180	10	σ,α	$^7F_6(E^{(3)})$-$^7F_0(A_1)$
4922	−180	7	σ,α	
4947	−180	10	π	$^7F_6(B_2^{(2)})$-$^7F_0(A_1)$
5053	−180	9	σ,α	$^7F_6(E^{(2)})$-$^7F_0(A_1)$
5071	−180	9	σ,α	$^7F_6(E^{(1)})$-$^7F_0(A_1)$
5139	−180	8	σ,α	

[a] The polarization and relative intensity are reported in the same manner as in Table I, except for the use of absorbance in place of emission.

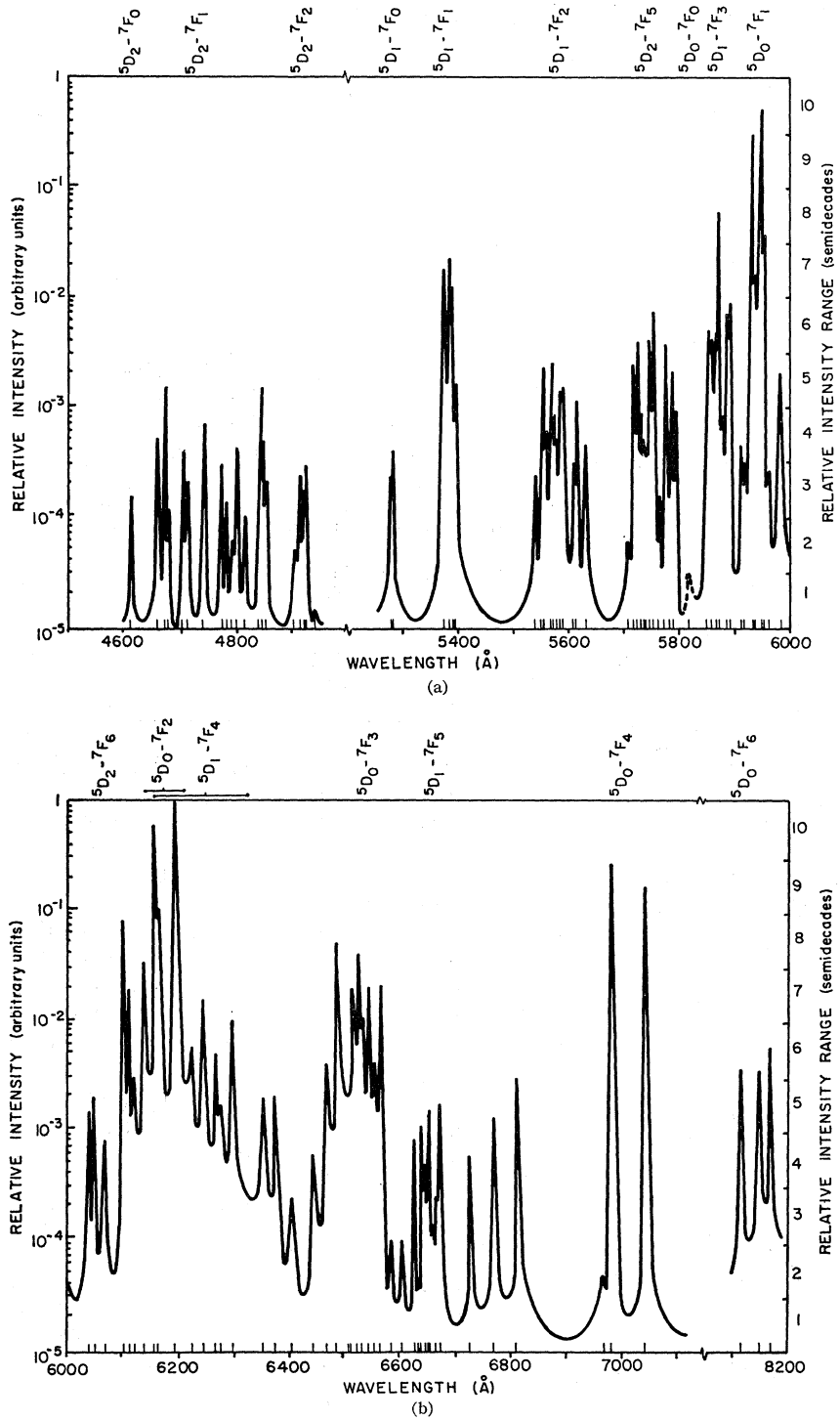

FIG. 1. Unpolarized fluorescence emission spectrum of europium-doped yttrium vanadate. Temperature is −180°C. The $^5D_0$-$^7F_0$ emission (broken curve) was observed in the powder only; all other emissions are from single crystals, with intensities averaged over all three crystal axes. See Table I, footnote a.

and 333.7 cm^{-1}, respectively. With this information and the observed magnetic-dipole emissions from the $^5D_0$-$^7F_1$ transitions, at 5935.1 and 5949.7 Å, the $^5D_0$ level can be unequivocally located at 17 183.2 cm^{-1}. Indeed an extremely weak emission at 5819 Å, corresponding to this assignment, can be just barely detected in the powder. We thus have a rough indication of how well the symmetry-determined selection rules hold in this material; the peak intensity of the forbidden transition is more than four orders of magnitude less intense than in the symmetry-allowed $^5D_0$-$^7F_2$ transition.

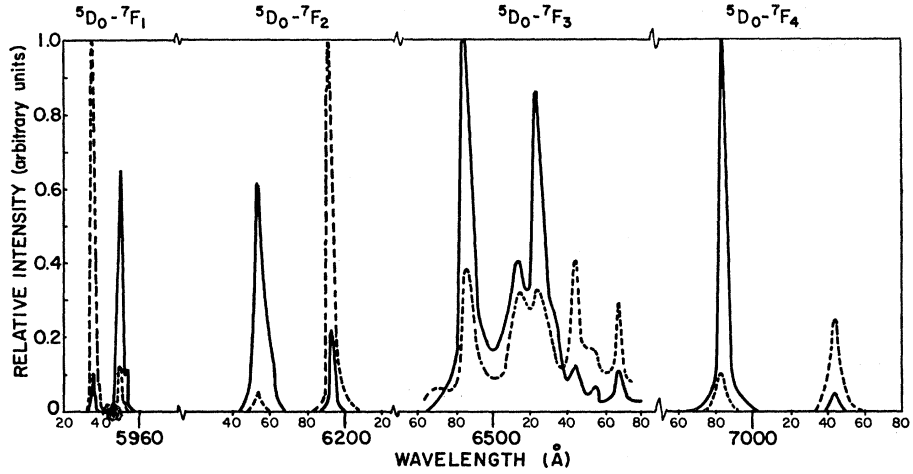

FIG. 2. Polarized fluorescence emissions originating from the $^5D_0$ state, as observed in the transverse crystal direction. Broken line, electric vector perpendicular to unique axis (σ spectrum); solid line, electric vector parallel to unique axis (π spectrum). Temperature is $-180°C$. Intensity scales normalized relative to strongest emission in each spectral region; for comparison between regions, multiply by the following factors: $^5D_0$-$^7F_1$, 0.5; $^5D_0$-$^7F_2$, 1.0; $^5D_0$-$^7F_3$, 0.05; $^5D_0$-$^7F_4$, 0.25.

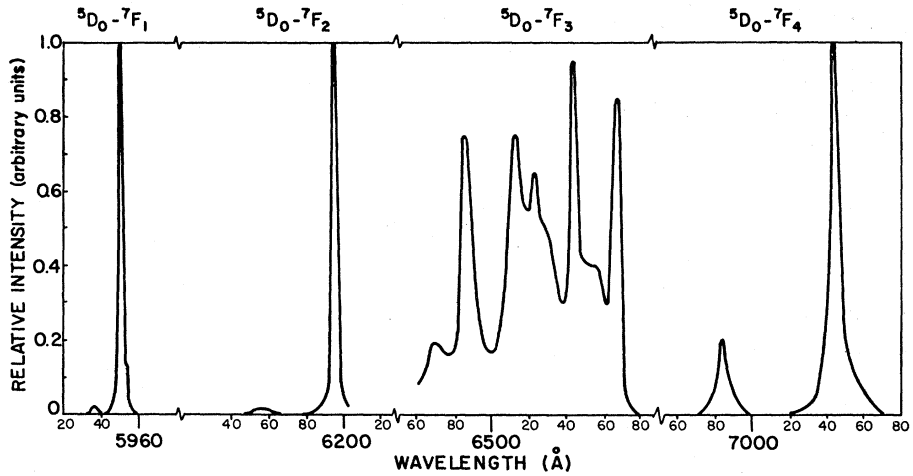

FIG. 3. Fluorescence emissions originating from the $^5D_0$ state, as observed in the axial crystal direction. Emitted light unpolarized (α spectrum). Temperature is $-180°C$. Intensity scales as in Fig. 2.

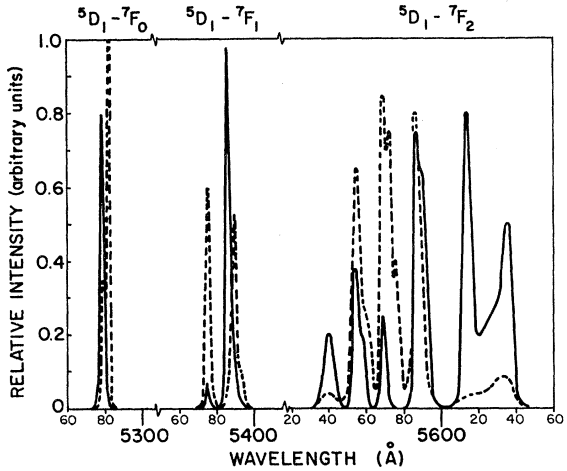

FIG. 4. Polarized fluorescence emissions originating from the $^5D_1$ state, as observed in the transverse crystal direction. Broken line, electric vector perpendicular to unique axis (σ spectrum); solid line, electric vector parallel to unique axis (π spectrum). Temperature is $-180°C$. Intensity scale factors: $^5D_1$-$^7F_0$, 4×10^{-4}; $^5D_1$-$^7F_1$, 2.5×10^{-2}; $^5D_1$-$^7F_2$, 2.5×10^{-3}.

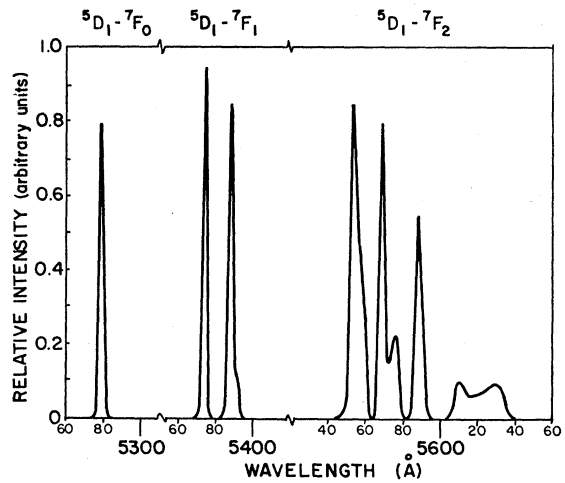

FIG. 5. Fluorescence emissions originating from the $^5D_1$ state, as observed in the axial crystal direction. Emitted light unpolarized (α spectrum). Intensity scales as in Fig. 4.

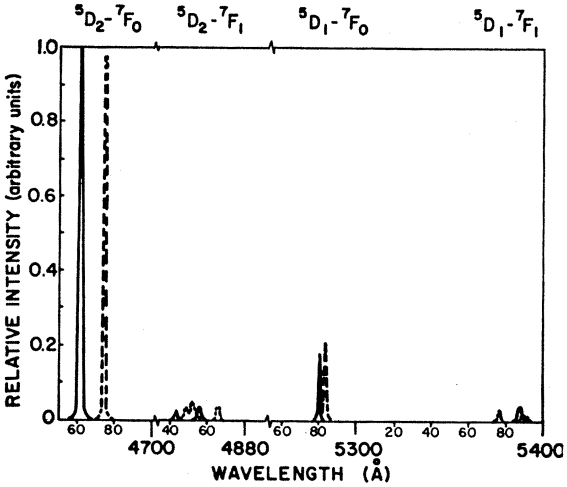

FIG. 6. Polarized absorption spectrum of europium-doped yttrium vanadate in the visible region, as observed in the transverse crystal direction. Broken line, electric vector perpendicular to unique axis (α spectrum); solid line, electric vector parallel to unique axis (π spectrum). Temperature is $-180°C$ for $^7F_0$ absorptions, $+25°C$ for $^7F_1$ absorptions. Intensity scale in absorbance relative to most intense transition.

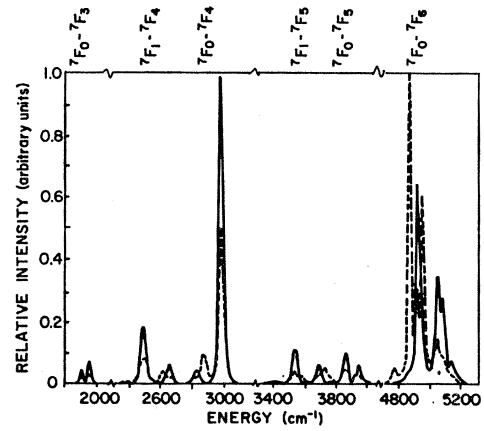

FIG. 7. Absorption spectrum of europium-doped yttrium vanadate in the infrared region. Solid line, observed in the axial crystal direction (α spectrum); broken line, observed in the transverse crystal direction ($\sigma+\pi$ spectra). Incident light unpolarized. Temperature is $-180°C$ for $^7F_0$ absorptions, $+25°C$ for $^7F_1$ absorptions. Intensity scale in absorbance relative to most intense transition. Background atmospheric and lattice absorptions not shown.

For the most part, the structure of the ^7F multiplet can be determined by analysis of the emission from the $^5D_0$ and $^5D_1$ states or of the infrared absorption from the $^7F_0$ ground state. The two $^7F_1$ levels have already been identified in the course of the measurement of the energy of the $^5D_0$ level. The next higher member of the ^7F multiplet is the $^7F_2$ which consists of four levels, three nondegenerate (A_1,B_1,B_2) and one degenerate (E). The B_2 and E levels can be identified from the $^5D_0$-$^7F_2$ emission, an electric-dipole transition, which shows a component polarized along the c axis at 6155.2 Å and a perpendicular component at 6193.8 Å. Transitions from the $^5D_0$ to the other two levels of the $^7F_2$ are optically forbidden, but those originating from the $^5D_1$ state are not; the latter transitions not only confirm the identification of the B_2 and E levels of the $^7F_2$, but locate the A_1 and B_1 components as well. The assignments are: $A_1=985.4$ cm^{-1}; $B_1=1116.1$ cm^{-1}; $B_2=936.4$ cm^{-1}; and $E=1038.7$ cm^{-1}.

The next higher state to be considered is the $^7F_3$, which consists of three nondegenerate and two doubly degenerate levels. The $^5D_0$-$^7F_3$ transition, following electric-dipole selection rules, should give rise to only three optically active components, in the 6500-Å region of the spectrum; in fact, four prominent emissions are found. Fortunately, however, only three show strong polarization character, one at 6524 Å parallel to the c axis and two, at 6545 and 6567 Å, perpendicular. Using this polarization as a criterion, we disregard as extraneous the line at 6487 Å (possibly arising from a higher-state transition or an impurity), and identify the B_2 and two E levels of the $^7F_3$ at 1854.8, 1904.0, and 1955.0 cm^{-1}. Corresponding emissions from the $^5D_1$ levels confirm these identifications (in particular, no

TABLE IV. Selection rules for electromagnetic transitions in D_{2d} symmetry.[a]

Representation of terminal state	Representation of initial state A_1	A_2	B_1	B_2	E
A_1		Mag: σ		Elec: π	Elec: σ,α Mag: π,α
A_2	Mag: σ		Elec: π		Elec: σ,α Mag: π,α
B_1		Elec: π		Mag: σ	Elec: σ,α Mag: π,α
B_2	Elec: π		Mag: σ		Elec: σ,α Mag: π,α
E	Elec: σ,α Mag: π,α	Elec: σ,α Mag: π,α	Elec: σ,α Mag: π,α	Elec: σ,α Mag: π,α	Elec: π Mag: σ

[a] In europium, all transitions for which $\Delta J\neq\pm1$ obey electric-dipole selection rules. Among the transitions for which $\Delta J=\pm1$, however, magnetic-dipole selection rules are obeyed only by those for which $J=0$ in either initial or terminal states. In the absence of the latter condition, all other transitions show a mixed character, to which both electric- and magnetic-dipole mechanisms contribute.

$^5D_1$ emission corresponding to the above-mentioned "extraneous" line can be found), and also indicate the locations of the missing members of the $^7F_3$ set. All these identifications are given further support by the results of the crystal-field calculation discussed later.

The next higher state, the $^7F_4$, has seven components, of which only three (one nondegenerate and two degenerate) are the terminal states of optically active transitions from the $^5D_0$ or $^7F_0$ states. Two of these levels, a B_2 at 2867.7 cm^{-1} and an E at 2988.4 cm^{-1}, can be unequivocally identified from both emission and absorption measurements. Evidence for the second E level is found in a weak infrared absorption at 2830 cm^{-1}, but corresponding evidence in the emission spectra is less certain. The emissions from the $^5D_1$ state, for once, fail to offer assistance in this regard, since the predicted location of the transitions terminating in the 2830-cm^{-1} E level fall in the midst of the much more intense $^5D_0$-$^7F_2$ transition at 6193.8 Å. The $^5D_1$ emissions do, however, make it possible to locate the B_1, the A_2, and both A_1 levels.

As for the $^7F_5$ state, transitions to it from the $^5D_0$ state are too weak to be seen in emission under the conditions of these experiments. The state has eight levels, of which four (B_2 and three E) are the terminal states of optically active transitions from the ground state. Only two of the degenerate states are found conclusively in infrared-absorption measurements, at 3949 and 3870 cm^{-1}, with some weaker evidence of the third E at 3928 cm^{-1} and a B_2 level at about 3915 cm^{-1}. Extremely weak emissions from the $^5D_1$ state terminating in some of the $^7F_5$ levels are also found. On the whole, however, the $^7F_5$ state is the least well defined from our data, and we have chosen not to use them in the determination of the crystal-field parameters but to reserve them as a check on the results.

The measurements on the $^7F_6$ state yield more complete information. Of the ten components of this state, three degenerate levels can be located from the infrared absorption, at 5071, 5053, and 4916 cm^{-1}, and two nondegenerate B_2 levels, at 4947 and 4867 cm^{-1}. The three lowest levels are confirmed by barely detectable emissions from the $^5D_0$ state, but no corresponding emissions from the $^5D_1$ state can be found. Despite the consequent inability to locate the other components of the $^7F_6$ state, enough information is known to allow its use in the calculations.

The assignments for all relevant energy levels are presented in Table V. The energies of the levels in the ^7F multiplet shall be used in the next section for the crystal-field calculations. Before proceeding to this, however, it would be pertinent to note that the observations of the various transitions are in excellent agreement with the theoretical symmetry-based selection rules. The rigorous predictions on the basis of a D_{2d} site, as listed in Table IV, are obeyed to a remarkable degree. The forbidden transitions are, to all intents and purposes, absent from the spectra. Most of the allowed transitions are observed. The polarization of the observed emissions and absorptions are satisfactorily complete (>5:1), within the experimental limitations. Not all of the detected optical transitions can be identified, but these are invariably weak ones for the region in which they appear, and can be ascribed to

TABLE V. Energy levels of Eu^{+3} in YVO_4 as split by the crystal field.

State	Component	Energy (cm^{-1}) observed[a]	Energy (cm^{-1}) calculated[b]	Approx. precision of fit $\langle\delta E/E\rangle_{av}$ (%)	Approx. precision of fit $\langle\delta E/\Delta E\rangle_{av}$ (%)
$^7F_1$	A_2	333.7	336.4	0.5	12.0
	E	375.6	372.9		
$^7F_2$	A_1	985.4	972.8	0.4	11.4
	B_1	1116.1	1123.5		
	B_2	936.4	937.2		
	E	1038.7	1043.1		
$^7F_3$	A_2	1873.0	1875.9	0.1	11.1
	B_1	1903.0	1908.9		
	B_2	1854.8	1853.1		
	$E^{(1)}$	1957.0	1951.6		
	$E^{(2)}$	1904.0	1902.2		
$^7F_4$	$A_1^{(1)}$	3063.0	3049.5	0.2	12.9
	$A_1^{(2)}$	2879.0	2882.1		
	A_2	2923.0	2903.3		
	B_1	2700.0	2697.0		
	B_2	2867.7	2864.8		
	$E^{(1)}$	2988.4	2999.2		
	$E^{(2)}$	2830.0	2855.0		
$^7F_5$	A_1	3800	3780	0.2	20
	$A_2^{(1)}$	3750	3765		
	$A_2^{(2)}$	3870	3875		
	B_1	4065	4030		
	B_2	3915	3915		
	$E^{(1)}$	3949	3975		
	$E^{(2)}$	3928	3935		
	$E^{(3)}$	3870	3860		
$^7F_6$	$A_1^{(1)}$		5131.6	0.3	30
	$A_1^{(2)}$		4959.6		
	A_2	5050	5051.9		
	$B_1^{(1)}$		5178.9		
	$B_1^{(2)}$		4933.0		
	$B_2^{(1)}$	4947	4945.1		
	$B_2^{(2)}$	4867	4868.9		
	$E^{(1)}$	5071	5120.9		
	$E^{(2)}$	5053	5048.0		
	$E^{(3)}$	4916	4953.5		
$^5D_0$	A_1	17 183.2			
$^5D_1$	A_2	18 932			
	E	18 941			
$^5D_2$	A_1	21 359			
	B_1	21 419			
	B_2	21 455			
	E	21 396			

[a] The observed energy levels were derived using only data obtained at −180°C, with room-temperature measurements serving only to confirm the assignments.

[b] The calculated energies were obtained by using the crystal-field parameters listed in Table VI. Since the $\bar{E}_n$ values, like the B's, are fitted parameters, and may deviate from the actual experimental mean energies by as much as 5 cm^{-1}, the precision of fit is given in terms of two quantities: the probable error in the total energy of the levels of a particular J state, $\langle\delta E/E\rangle_{av}$, and the probable error in the Stark shift of those levels from the mean energy of that J state, $\langle\delta E/\Delta E\rangle_{av}$.

transitions from higher states, to impurities, or to crystal imperfections.

Crystal-Field Calculations

The calculation of the crystal-field parameters is carried out under the same rules as have been proven valid for the identification of the spectroscopic data. The cardinal tenets of this treatment are that the crystal field operate only on the J number of the particular level, and that the resultant splitting of each J level be significantly less than the spacing between different J levels. These conditions, although demonstrably valid for all europium levels (both ^5D and ^7F) studied, must now be fortified with three additional restrictions. The first is that the crystal-field interaction be essentially electrostatic in character, with no significant covalency or other effects. This is generally the case in rare-earth ions anyway, and is all the more so in the ionic YVO_4 lattice. The second requirement is that the degree of orbital coupling between the multiplet under consideration and others be small; that is, that states in the ^7F multiplet, for example, have essentially no admixture of the ^5D or other non-^7F states. It is for this reason that we cannot treat the ^5D multiplet in the same manner as the ^7F, since the former has at least 25–30% mixture of "foreign" states as against only 3–4% for the latter.[15] Finally, we require that the amount of J mixing between levels in the same multiplet be similarly negligible. The validity of the simple crystal-field model diminishes as the magnitude of such mixing increases, and the discrepancies between measured and calculated energy levels can be ascribed largely to this effect.

The splitting of each of the ^7F levels can be expressed in terms of the crystal-field contribution to the Hamiltonian for the system. This crystal-field Hamiltonian H_c is most conveniently written in the operator-equivalent form

$$H_c=\sum_n \sum_m \theta_j^n[B_{nm}^c O_{nm}^c+B_{nm}^s O_{nm}^s], \qquad (1)$$

where $B_{nm}=A_{nm}\langle r^n\rangle=-|e|K_n\langle r^n\rangle\gamma_{nm}$ are the familiar "optical parameters"; $O_{nm}^{c,s}$ are the operator-equivalent expressions; θ_j^n is the operator-equivalent factor α_j, β_j, or γ_j; and K_n is a normalizing factor. The problem is then to solve the secular equation for each J, given the form of H_c. The various entries in the secular determinant are

$$\langle JM|H_c|JM'\rangle=H_{MM'} \qquad (2)$$

and these are readily evaluated from published tables.[16] The maximum advantage of group theory is obtained by using symmetry-adapted functions, which automatically achieves a maximum simplification of the secular equation. The details of such calculations for various octacoordinate symmetries are given in a separate paper.[17]

TABLE VI. Calculated crystal-field parameters for Eu^{+3} in YVO_4.

Parameter	Value (cm^{-1})	Approx. precision[a] (%)
$\bar{E}_1$	360.8	±0.4
$\bar{E}_2$	1023.9	±0.1
$\bar{E}_3$	1906.5	±0.02
$\bar{E}_4$	2900.6	±0.25
$\bar{E}_5$	(3900)[b]	
$\bar{E}_6$	5024.1	±0.3
B_{20}	−61.0	± 25
B_{40}	+50.4	± 14
B_{60}	−60.1	± 6
B_{44}	−733.3	± 5
B_{64}	+27.8	±100

[a] This precision measure is derived from the approximate range of variation exhibited by each parameter, as produced when various random sets of experimental points are omitted from the fitting procedure.
[b] Since no $^7F_5$ levels were used in the computation of the crystal-field parameters, the mean energy for this group could not be obtained thereby. The $\bar{E}_5$ value listed was calculated afterwards, using the available data and the other fitted parameters.

The D_{2d} symmetry of the YVO_4 lattice simplifies the calculations considerably, and the resultant Hamiltonian, which contains only cosine terms, requires the determination of only five crystal-field parameters (B_{20}, B_{40}, B_{44}, B_{60}, and B_{64}). These five, plus the mean energies of each J state, make a total of eleven unknown quantities needed to describe the crystal-field splitting of the ^7F multiplet. To determine these parameters we have a total of 23 experimentally determined energies, so that the system of equations resulting from the solution of the secular determinant is considerably overdetermined. Since not all of the experimental values are known to the same high degree of confidence, we use the following procedure to find the best fit.

As a first step, an initial set of the five optical parameters is obtained by utilizing only those experimental values known to the greatest confidence. These points are the two $^7F_1$ levels, the B_1, B_2, and E levels of the $^7F_2$, the B_2 and two E levels of the $^7F_3$, and the B_2 and higher E levels of the $^7F_4$. This results in a number of possible sets of parameters because of the inherent ambiguity in the solution of quadratic equations. The remaining data are then used to select the physically meaningful set. With this as a starting point, a computer program is employed to fit the parameters with all of the 23 sufficiently well-known energies, producing a best set of values according to a least-squares criterion. This set is then used to calculate all other energies not used, as a check on the theory. The observed and calculated energies and the final crystal-field parameters are given in Tables V and VI.

The results of the crystal-field calculations reveal a number of points of significance. One of those, readily

[15] G. S. Ofelt, J. Chem. Phys. 38, 2171 (1963).
[16] M. T. Hutchings, in *Solid State Physics*, edited by F. Seitz and D. Turnbull (Academic Press Inc., New York, 1964), Vol. 16, p. 227.
[17] A. Lempicki, H. Samelson, and C. Brecher (to be published).

seen from the reported precision measures, is that the crystal-field parameters are relatively insensitive to small errors in the assignment of energies and to the inclusion or omission of some of the experimental points. Indeed, all but one (B_{64}) of these parameters[18] are within 20% of the initial values found without a computer fit, and the omission of any of the less certain assignments ultimately results in calculated values within 20 cm^{-1} of the levels in question. The over-all fit of the 36 Stark levels is, with few exceptions, equally satisfactory, and the over-all precision measure of the fit, expressed in terms of the total energy of each level, is better than 0.3%.

This precision measure, unfortunately, does not give a true picture of the applicability of the crystal-field approximation. A far better procedure would be to disregard the fact that the mean energies of each ^7F level are also fitted parameters and to express the probable deviation not in terms of total energy but rather in terms of the most probable displacement of a given level from the mean energy of the ^7F set to which it belongs. In these terms the over-all precision measure of the fit is on the order of 15%, a respectable value in view of the crudeness of the crystal-field treatment used. The major portion of this deviation presumably arises from the neglect of the J-J interactions, and the precision of fit should be improved markedly by inclusion of the suitable coupling terms. The contribution of other factors, such as an admixture into the f shell of the other orbitals, remains undetermined here and must await a more comprehensive treatment using the more refined ligand-field model.

Another interesting point is found upon examination of the algebraic signs of the optical parameters B_{nm}. Within the set, the relative signs are completely consistent with what would be predicted on the basis of the known geometrical arrangement (D_{2d}) of the oxygens surrounding the europium. In a study of europium in another type of octacoordinate lattice, the garnet, Koningstein[9] found sets of crystal-field parameters whose signs are equally consistent internally with the oxygen arrangement in that lattice (D_2). Upon comparing the two sets of parameters with each other, however, one immediately sees that despite the internal consistency of each set, each parameter we find for the zircon has the opposite sign from the corresponding one found for the garnet.[19]

This discrepancy in sign is puzzling. It seems unlikely that the mere difference in symmetry (D_2 versus D_{2d}) would be enough to explain the sign change, since the actual arrangements of oxygens are derived from the dodecahedral in both cases.[20] The possibility of error of assignment cannot be overlooked, particularly since the absence of polarization in the garnet spectrum precludes the use of such data to remove the inherent ambiguity in the completely split europium levels, but the internal consistency of the data argues against this. Finally, a speculative but more interesting possibility is that the discrepancy may arise from differences in the chemical interactions of the europium with its surroundings, perhaps involving changes in the degree of covalency of the europium-oxygen bonds or some more subtle shielding effect. The problem of relating the crystal-field model with the chemical properties of the lattice is not simple, and merits more study.

CONCLUSION

The polarized fluorescence emission and absorption spectra of Eu^{+3} in YVO_4 have yielded a reasonably complete and consistent picture. Most of the observed transitions have been assigned and an energy-level structure has been obtained for the complete F multiplet, and for the first three members of the excited ^5D multiplet as well. Elementary crystal-field theory has been applied to the ^7F multiplet and the set of optical parameters thereby obtained yields a satisfactory agreement between the observed and calculated Stark levels. The signs of the parameters obtained for europium in the YVO_4 structure are the direct opposite of those found in garnets, although the reason for this remains unclear. On the whole, however, the crystal-field treatment does appear in this case to give a good approximation to reality.

ACKNOWLEDGMENTS

The authors wish to express their appreciation to S. Barton for his valuable contributions in the computer programming and to K. W. French and A. Rogall for their assistance during the course of the experiments.

[18] The B_{64} parameter is the least precise of those determined here, since it is almost invariably coupled in the crystal-field equations with the much larger B_{44} term. Consequently, even fairly large deviations in this parameter do not have a substantial effect on the quality of the fit.

[19] With the occasional exception of the aforementioned B_{64} term.

[20] The behavior and relative signs of the crystal-field parameters can be calculated on purely geometrical grounds. Such calculations indicate that the systematic distortions of the oxygens required to transform one of these geometrical arrangements into the other are not sufficient to change the signs of all parameters while still maintaining the same internal relationship within the set. This will be discussed in a separate paper (Ref. 17).